LD01

19th International Symposium of Ballistics, 7–11 May 2001, Interlaken, Switzerland

SABOT DISCARD MODEL FOR CONVENTIONAL AND ELECTROMAGNETIC LAUNCH PACKAGES

Mehmet E. Erengil

Institute for Advanced Technology, 3925 West Braker Lane, Suite 400, Austin, TX, USA

This paper presents the sabot discard model, which has recently been developed at the Institute for Advanced Technology to predict sabot separation for conventional and electromagnetic launch packages. The model uses analytical expressions to estimate transient surface pressure distributions, which are then integrated numerically to determine petal trajectories. The most significant attribute of this model is that it does not rely on any empirical data and is therefore expected to be widely applicable. Good comparisons between measured and predicted surface pressure distributions suggest that the important aerodynamic features of sabot separation process have been captured by the model. More importantly, however, comparisons between measured and predicted sabot petal trajectories æ for radial as well as angular displacements æ show that model predictions are excellent for both conventional and electromagnetic launch packages.

INTRODUCTION

It is well known [1] that aerodynamic and mechanical interference during sabot discard can adversely affect the trajectory of the sub-projectile resulting in loss of accuracy and a significant increase in round-to-round dispersion. Thus, reliable sabot discard models are required to predict the effect of sabot separation on sub-projectile trajectories in direct fire applications. However, the complex aerodynamic interactions (e.g., transient shock/shock and shock/boundary-layer interactions) occurring during sabot discard have precluded the development of accurate and widely applicable models. Due to the lack of reliable models, the trajectory analysis codes tend to use experimental measurements and/or empirical estimates to account for the effect of sabot discard on sub-projectile trajectories.

Earlier modeling efforts [2–4] resulted in the development of the AVCO code, which relied on empirical data for estimating surface pressure distributions and has therefore had limited accuracy and applicability. This limitation was also observed in previous studies conducted at the Institute for Advanced Technology (IAT) [5, 6]. More recently [7, 8], the IAT has begun a systematic study to develop a sabot separation model that could

ultimately be integrated into trajectory analysis codes to help address the effects of sabot discard on accuracy and dispersion for both conventional and EM-launched projectiles.

The objectives of this paper are to summarize the IAT sabot discard model, validate the model predictions with wind tunnel measurements and compare measured and predicted sabot petal trajectories in both conventional and electromagnetic launch.

THE AERODYNAMIC MODEL

To better model the complex aerodynamic interactions occurring during sabot discard, the transient process is divided into four phases. In each phase, at each instant in time, surface pressure distributions are estimated using relatively simple analytical relations, which are integrated to yield forces and moments on the petals at that instant. The resultant axial, radial and angular accelerations are then integrated again, in a time-marching algorithm, to determine radial and angular trajectories of sabot petals. For most cases of interest, the effect of the projectile bow shock on surface pressure distributions on sabot petals is negligible and can therefore be neglected. Surface pressures on all leeward surfaces are assumed to be equal to the incoming freestream pressure. Furthermore, since the sabot discard occurs within a relatively short distance from the muzzle, the incoming Mach number can be assumed to be constant.

Phase I: Choked Flow

In this phase (see Fig. 1a), the flow is choked since the gap between the petals is not large enough to accommodate the incoming mass flow rate. The interaction is characterized by a single normal shock upstream of the sabot petals and essentially a stagnant volume of air within the scoop. The subsonic flow behind the normal shock is accelerated to supersonic Mach numbers as it turns through a series of expansion waves and aligns itself with the petal interfaces surrounding the core flow. (This is similar to subsonic flow in a converging channel, which has to accelerate.) However, since the area between the petals continues to decrease, the supersonic flow will terminate in a second normal shock called the throttling shock. This phenomenon has also been observed in the surface pressure distributions measured in wind tunnel experiments (see Fig. 2b). The location of the throttling shock depends on the area ratio and the Mach number of the supersonic flow between the petals. The area ratio can be calculated from the radial position and angle-of-attack of the petal at that instant in time. Mach number, on the other hand, can be calculated by estimating the local static pressure, using hypersonic relations based on blast wave theory, and assuming isentropic expansion from stagnation conditions behind the first normal shock upstream of the entire package. The flow through the launch package remains choked until the area between the petals is large enough to accommodate the incoming mass flow rate.

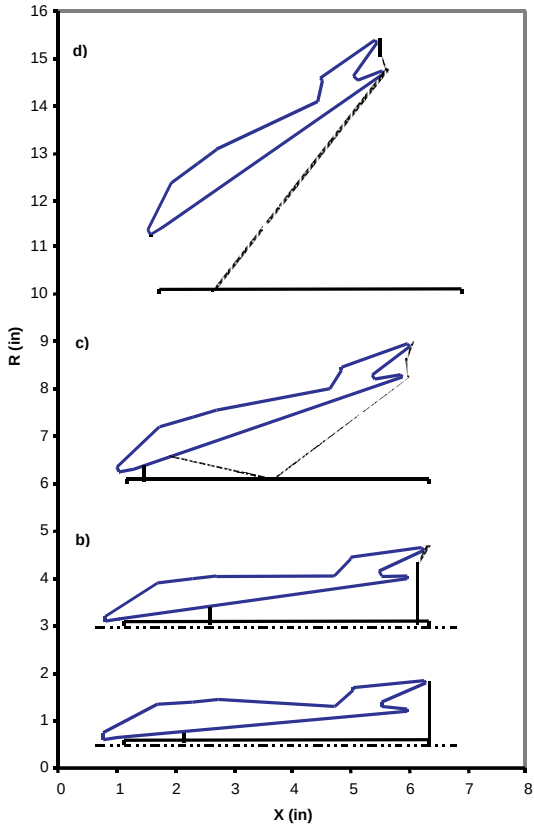

Figure 1. The Aerodynamic Model. a) Phase I: Choked flow, b) Phase II: Normal shock convection, c) Phase III: Oblique shock convention, and d) Phase IV: Free flight.

Phase II: Normal Shock Convection

In this phase (see Fig. 1b), the flowfield structure is fundamentally the same as that in Phase I except that the normal shock upstream of the launch package begins to move downstream. During this phase, the flow structure near the leading edge of the sabot changes from a single normal shock into a system of multiple bow shocks, each emanating from an individual sabot petal. This evolution results in a bimodal pressure distribution within the scoop, which has also been observed in surface pressure distributions measured in wind tunnel experiments (see Fig. 2c). The speed of the normal shock convection can be estimated from the rate at which the stagnant mass of air within the scoops is depleted. Surface pressures and the throttling shock parameters are estimated as in Phase I. It should be noted that while the duration of Phase II is typically very short, this phase could have a significant effect on petal trajectories depending on the details of sabot design.

Phase III: Oblique Shock Convection

In this phase (see Fig. 1c), the flow structure is characterized by multiple bow shocks, each emanating from the petal leading edge, and oblique shocks, which reflect off of each other in symmetry plane(s) and also from the surface of the sub-projectile. The flow properties across the oblique and reflected shocks are calculated from two-dimensional compressible flow relations. Depending on the instantaneous flow conditions and the particular configuration, the throttling shock may or may not exist. If it does exist, then flow conditions downstream of the reflected shock are used to determine the throttling shock location along the petal.

Phase IV: Free Flight

In this phase (see Fig. 1d), the flow structure for each petal is characterized by a bow shock emanating from the petal leading edge. The petals have rotated and displaced sufficiently far apart that the reflected shocks will no longer intersect with the petals. In other words, the petals have entered free flight. It should be noted that the sub-projectile does not enter free flight until the bow shock, emanating from each petal no longer interacts with the sub-projectile. Again, the surface pressures on windward sides of sabot petals are estimated from relatively simple analytical relations as before.

DISCUSSION OF RESULTS

Surface Pressure Distributions

A series of experiments were conducted [6] at the Mach 5 Wind Tunnel Facility of The University of Texas at Austin to measure the mean surface pressure distributions along the windward side of a typical conventional sabot petal. Since the test section could only accommodate one petal, the symmetry condition was achieved by mounting thin splitter plates along the sub-projectile in the interface planes. Four different configurations were tested, each corresponding to the ‘steady-state’ conditions at that instant during discard. Results from two test configurations are presented below.

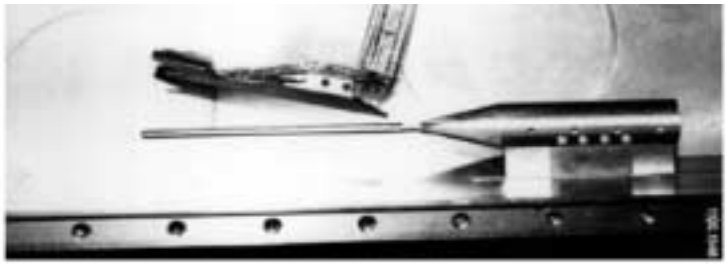

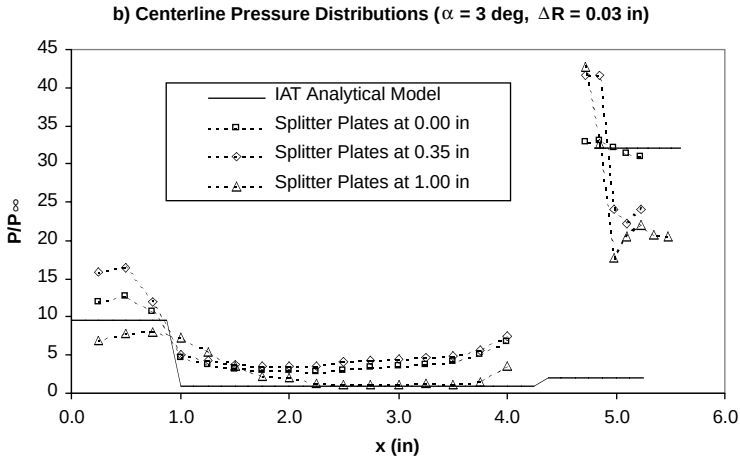

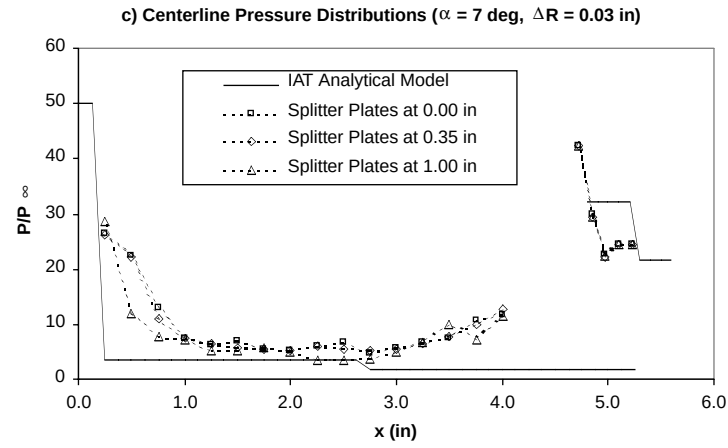

Figure 2. Surface Pressure Distributions. a) Wind tunnel model (the flow is from left to right), and Comparison of measured and predicted pressure distributions along the center-line (the flow is from right to left) for b) α = 3 deg., ΔR = 0.03 in, and c) α = 7 deg., DR = 0.03 in.

Figure 2a shows a photograph of the test setup without the splitter plates; the flow is from left to right. Figures 2b and 2c show the comparison of measured and predicted surface pressure distributions along the centerline of the sabot petal at α = 3-deg. and 7-deg., respectively. Note that in Figs. 2b and 2c the flow is from right to left. In both test configurations, the tail of the sabot was 0.03 in from the sub-projectile. Very high surface pressures within the scoop and also near the tail of the petal are evident in both cases. The high pressures near the tail are due to the throttling shock as was discussed earlier. These results show that the agreement between model predictions and the wind tunnel measurements is fairly good, suggesting that the relatively simple model has indeed captured the important aerodynamic features of this very complex and transient interaction. The model not only predicts the location but also the amplitude of the pressure rise. Furthermore, it also predicts the bimodal pressure distribution within the scoop, which is due to the normal shock convection as was discussed earlier.

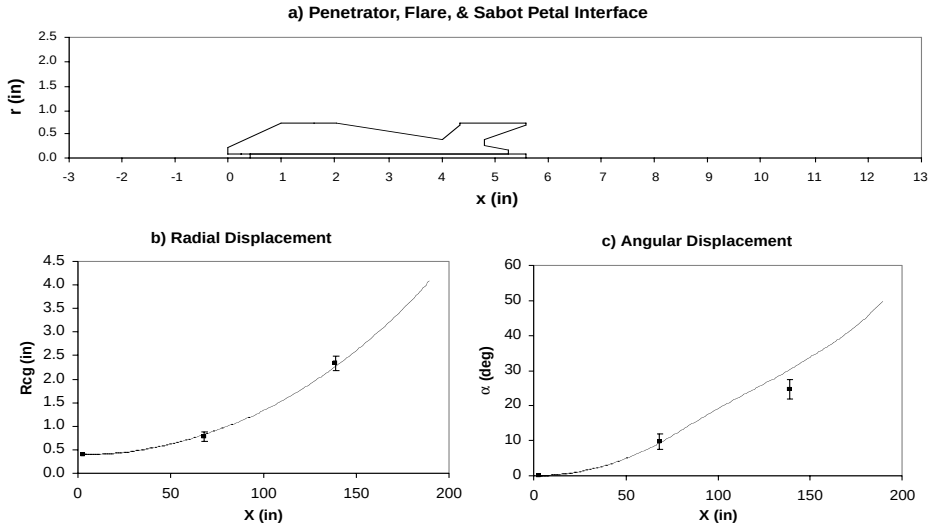

Figure 3. Conventional Launch. a) Penetrator and sabot interface, b) Radial displacement, and c) Angular displacement trajectories.

Sabot Discard for Conventional Launch Packages

Figures 3 and 4 show the comparisons of sabot petal trajectories (both radial and angular) with flight data obtained at the IAT's two-stage light-gas gun facility for two significantly different launch package designs. The schematics above the trajectory data show the cross-section of the assembled package at launch and also serve to highlight the differences between the two launch packages. While the range data are limited, the agreement between the experimental data and the model predictions is very good for both cases showing the applicability of the sabot discard model to a relatively wide range of designs. This can be attributed to the fact that the IAT model does not rely on any empirical data for its predictions.

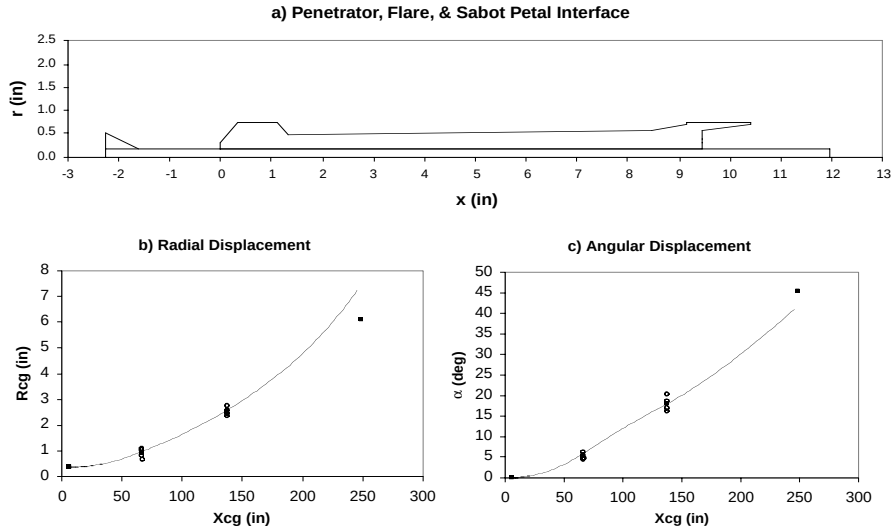

Figure 4. Conventional Launch. a) Penetrator and sabot interface, b) Radial displacement, and c) Angular displacement trajectories.

Sabot Discard for Electromagnetic Launch Package

Figure 5 shows the comparison between the actual armature/sabot petal trajectory data and model predictions for an electromagnetic (EM) launch package. Again, the schematic in Fig. 5a shows the interface of a two-petal armature/sabot; the discard plane is into the paper. The experimental data were obtained at the U. S. Army Research Laboratory Transonic Experimental Facility at Aberdeen Proving Ground, MD. A total of 5 shots were conducted at a nominal velocity of 1350 m/s.

An important feature of EM launch is the electromagnetic energy that is stored in the armature/sabot during launch. The stored magnetic energy remains within the launch package even after exit from the launcher. Upon exit, as the transport current is disengaged from the armature/sabot, induced currents begin to flow within the package until the residual magnetic energy decays to zero. The induced current and the magnetic field in the armature/sabot are oriented in such a way that the resultant force restrains the armature/sabot halves from separating in flight [9], thereby delaying discard. To a first order, the magnitude of this force scales with the magnitude of the peak transport current squared, and can be estimated from the transport current at exit and armature/sabot geometry [9]. In this case, however, the EM restraining force was determined experimentally in a separate study [10] and then incorporated into the sabot discard analysis. To assess the effect of EM launch on armature/sabot discard, the predicted trajectories were calculated with and without the EM restraining force.

These results show that the predictions of both radial and angular trajectories of armature/sabot petals are excellent. Furthermore, the IAT's sabot discard model demonstrates quantitatively the delayed armature/sabot discard caused by the EM restraining force.

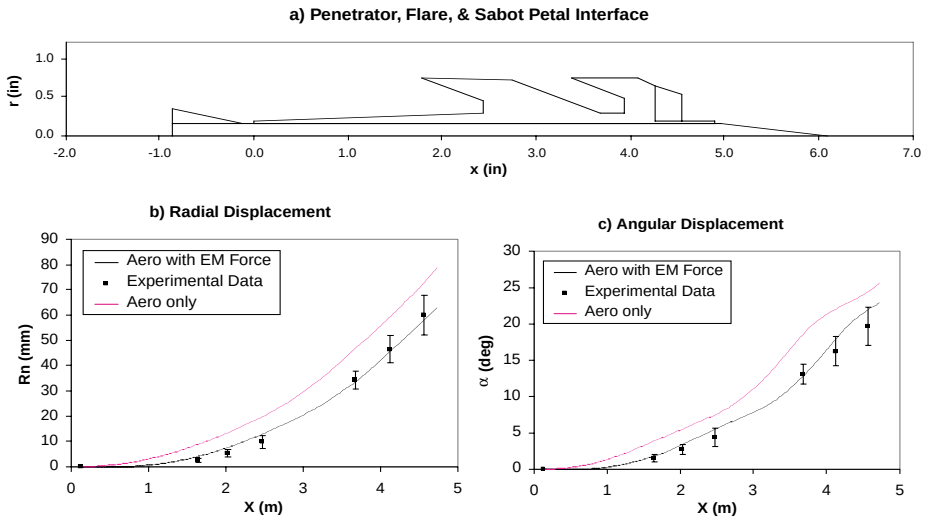

Figure 5. Electromagnetic Launch. a) Penetrator and armature/sabot interface, b) Radial displacement, and c) Angular displacement trajectories.

SUMMARY AND CONCLUSIONS

The sabot discard model, which was recently developed at the IAT to predict sabot separation for both conventional and electromagnetic launch packages, has been presented. The most significant attribute of this model is that it does not rely on any empirical data for its predictions. The model uses analytical expressions to estimate transient surface pressure distributions, which are then integrated numerically to determine petal trajectories. Fairly good comparisons between measured and predicted surface pressure distributions suggest that the aerodynamic model has indeed captured the important aerodynamic features of the complex, sabot separation dynamics. More importantly, comparisons between measured and predicted sabot petal trajectories for both radial and angular displacements show that model predictions are excellent for both conventional and electromagnetic launch.

ACKNOWLEDGEMENTS

This work was supported by the U.S. Army Research Laboratory under Contract DAAA21-93-C-0101.

REFERENCES

1. E. M. Schmidt and D. D. Shear, "Aerodynamic interference during sabot discard," *AIAA Journal of Spacecraft and Rockets*, Vol. 15, No. 3, 162–167, May–June 1978
2. P. Crimi and D. Siegelman, "Projectile/sabot discard aerodynamics," ARBRL-CR-00410, U.S. Army Ballistic Research Laboratory, Aberdeen Proving Ground, MD, December 1979
3. E. M. Schmidt, "Wind tunnel measurements of sabot discard aerodynamics," *AIAA Journal of Spacecraft and Rockets*, Vol. 18, No. 13, 235–242, May–June 1981
4. D. Siegelman, J. Wang, and P. Crimi, "Computation of sabot discard," ARBRL-CR-00505, U.S. Army Ballistic Research Laboratory, Aberdeen Proving Ground, MD, February 1983
5. M. J. Guillot and W. G. Reinecke, "A numerical and experimental investigation of sabot separation dynamics," IAT.R 0074, Institute for Advanced Technology, Austin, TX, September 1995
6. M. J. Guillot, J. N. Dick, and W. G. Reinecke, "Pressure distribution on sabots in hypervelocity flight," *AIAA Journal of Spacecraft and Rockets*, Vol. 34, No. 3, 279–284, May–June 1997
7. M. E. Erengil, "An aerodynamic model for symmetric sabot separation," AIAA Paper No. 99-0992, 37th Aerospace Sciences Meeting and Exhibit, Reno, NV, January 11–14, 1999
8. M. E. Erengil and A. E. Zielinski, "Effect of electromagnetic launch on armature/sabot discard," to be published in the *IEEE Trans. Magn.*, Vol. 37, No. 1, January 2001
9. S. Seiler, H. H. Legner, M. Miller, and W. G. Reinecke, "Intermediate ballistics model for hypervelocity projectiles launched from EM guns," *Proceedings of the 15th International Symposium on Ballistics*, Vol. 3, 291–298, Jerusalem, Israel, May 1995
10. E. Zielinski, P. Weinacht, and J. Bennett, "Electromagnetic and aeromechanical analysis of sabot discard for railgun projectiles," *AIAA Journal of Spacecraft and Rockets*, Vol. 37, No. 2, 257–264